Design and Test Results of an Actively Shielded Superconducting Magnet for Magnetic Resonance Imaging

Hong-Beom Jin, Kang-Sik Ryu, Bong-Hwan Oh, Kyung-Woo Ryu, and In-Young Jeong

Abstract

In this paper, we have studied about design and fabrication of the actively shielded superconducting MRI magnet. Nonlinear optimization methods are usually used to find optimum coil configurations. However the selection of initial coil configurations is very difficult. In case bad initial data are used, it is even impossible to find optimum coil configurations which satisfy predefined constraints. We have developed computer optimization program which consists of two steps. Initial coil configurations are easily selected through linear optimization in the first step and optimum coil configurations are found through nonlinear optimization in the second step. We have also studied about superconducting shim coils to cancel error fields caused by coil fabrication errors. Many researchers published design concepts of shim coil. However all these studies are for shim coil design using filamentary coils with single turn. Shim coils with multi-turns should be used to produce enough field strength to cancel error fields. We have developed computer program for the design of shim coils which have proper thickness and length. An actively shielded superconducting MRI magnet with a small warm bore was fabricated and four sets of superconducting shim coils were equipped. The magnetic field distributions were measured and field correction was carried out using shim coils.

I. Introduction

Superconducting MRI magnets should be shielded to prevent environment from strong stray fields[1]. Two major magnetic shield methods are commonly used. One is passive shield using ferromagnetic material around the magnet as a flux return path[2~5]. The other is active shield in which a magnet is shielded by incorporating a group of coaxial coils carrying current in the opposite direction to the main coil[6~9]. This arrangement reduces the stray field by diverting most of flux into the space between the main and shield coils. In passive shield, heavy iron is placed symmetrically around the magnet cryostat and increases the system weight too much causing the limitation of magnet siting. In active shield, shielding can be accomplished with minimum increase in system weight and flexibility of magnet siting is increased. This siting flexibility makes active shielding an attractive design alternative. However, very complicated computer optimization programs with constraints on stray field limits as well as on field homogeneity have to be developed to design actively shielded MRI magnet. The magnetic forces associated with active shielding magnet are generally twice those in a conventional magnet of the same field strength[7]. Therefore the structure supporting the coils must have sufficient strength and reliable magnet fabrication method have to be developed. we have studied about design and fabrication method of actively shielded superconducting MRI magnet.

M. Fujita[8] and A. K. Kalafala[9] published detailed studies about design method of actively shielded magnet. They suggested nonlinear optimization programs which allow search for optimum coil configurations under constraints on stray field limits and field homogeneity. In their program, initial coil configurations are roughly selected by imposing spatial restrictions and optimum coil configurations which satisfy imposed constraints with minimum conductor amounts are searched. However this kind of method requires repetitions of calculation very much times because initial data are too roughly selected. Selection of initial data with narrow bounds to reduce repetition times is very difficult and depends upon the designer's experiences.

We have developed computer optimization program which consists of two steps. Initial coil configurations are easily selected through linear optimization in the first step and optimum coil configurations are found through nonlinear optimization in the second step. We have fabricated an 1 Tesla actively shielded superconducting MRI magnet to confirm the validity of our design methods.

In designing MRI magnet which produce highly homogeneous magnetic field, only principle axial gradients of even order are

Manuscript received June 30, 1997; accepted November 13, 1997.

H. B. Jin and K. S. Ryu are with Korea Electrotechnology Research Institute, Changwon, Korea.

B. H. Oh is with Dept. of Electrical Engineering, MyongJi College, Korea.

K. W. Ryu is with the Dept. of Electrical Engineering, Chonnam National University, Korea.

I. Y. Jeong is with the Dept. of Electrical Engineering, Doo-won Technical College, Korea.

considered and multiple solenoid coils are properly arranged to cancel up to 8th or 10th order gradients. However, coil fabrication errors and ferromagnetic objects around magnet generate lower order gradients. These lower order gradients should be eliminated to achieve required homogeneity of $10^{-5}\sim10^{-6}$. Therefore, a field correction known as shimming is necessary.

We have also designed and fabricated superconducting shim coils to cancel error fields caused by coil fabrication errors. Many researchers[10~13] published design concepts of shim coil. However all these studies are for shim coil design using filamentary coils with single turn. Shim coils with multi-turns should be used to produce enough field strength to cancel error fields. We have developed computer program for the design of shim coils which have proper thickness and length.

In this paper, the optimum design programs of actively shielded superconducting MRI magnet and superconducting shim coil are presented. The details about magnet fabrication and field test are described.

II. Design of Magnet

1. Main Coil and Shielding Coil

In a spherical coordinate system(r, θ, φ) the magnetic field in the z-direction is defined as follows[12];

$$B_z = \sum_{n=o}^{\infty}\sum_{m=o}^{m=n} r^n [A^m_{n+1}\cos m\psi + B^m_{n+1}\sin m\psi]\times [(n-m+1)\cos\theta P^m_{n+1}(\cos\theta)+\sin\theta P^{m+1}_{n+1}(\cos\theta)] \quad (1)$$

where m and n are integers and A^m_{n+1} and B^m_{n+1} are arbitrary constants which will be determined by boundary conditions. $P^m_n(\cos\theta)=\sin\theta^m(\partial^m/\partial\cos\theta^m)P_n(\cos\theta)$ are associated Legendre functions.

In case of cylindrical symmetry, the magnetic field produced at a point with a spherical radius r and a colatitude angle θ by a current source is expressed as

$$Bz=\sum_{n=0}^{\infty} q_n r^n P_n(\cos\theta) \quad (2)$$

where $P_n(\cos\theta)$ is the Legendre polynomial of order n. In equation (2), the components $q_n=\frac{1}{n!}\frac{\partial^n B_Z(0)}{\partial Z^n}$ are known as the source terms of order n of a coil and dependent on the characteristics of the source coil. The components $r^nP_n(\cos\theta)$ are coordinate terms which determine the field point on the surface of a sphere. Using these terms for a solenoid coil symmetric to z=o plane, one can rewrite equation (2) as

$$Bz=B_0+q_2r^2P_2(\cos\theta)+q_4r^4P_4(\cos\theta)+\cdots\cdots \quad (3)$$

where B_0 is central field.

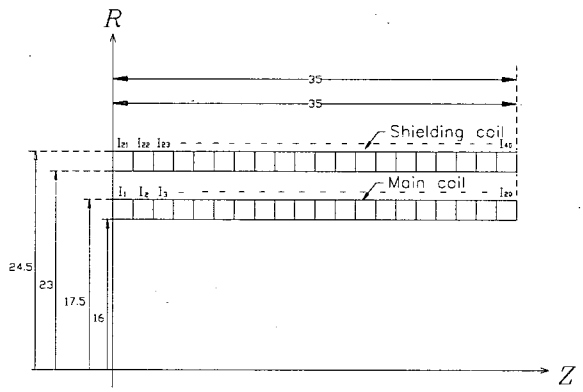

Fig. 1. Element division.

A field homogeneity of a magnet is normally defined as

$$\text{Homogeneity}=\frac{\triangle B}{B_0} \quad (4)$$

where $\triangle B=B_z(r,\theta)-B_0$ is field deviation from the central field over a given volume. Thus, in equation (3) the other terms except B_0 can be regarded as error field. If one arrange a set of solenoid coils symmetrically to z=o plane, then the field deviation due to the coils can be expressed as the sum of even order field harmonics.

$$\triangle B=\sum_{s=1}^{k} q_2^s r^2 P_2(\cos\theta)+\sum_{s=1}^{k} q_4^s r^4 P_4(\cos\theta)+\cdots\cdots \quad (5)$$

where k is the number of solenoid coils. The optimum coil arrangement that will generate a minimum field deviation can be selected by making the sum of even order source terms almost zero($\sum_{s=1}^{k} q_n\simeq 0$) up to some defined maximum order. It is possible to find optimum geometrical configuration and location of coils by computer program.

We have developed a computer optimization program for the design of an actively shielded MRI magnet. This computer optimization program consists of two steps. In the first step, initial geometrical configuration and location of coils are determined by a linear optimization. And then, optimum coil dimensions are selected by a nonlinear optimization in the second step.

Fig. 1 is the element division shown in 1/4 plane of the whole figure. The input coil dimensions are written in cm unit.

For an actively shielded superconducting MRI magnet, the most important parameter determining the amount of conductor and hence system cost is the gap length between inner radius of main coil and that of shielding coil. As the gap length increases, the amount of conductor decreases but the cryostat diameter should be increased[6]. It is the usual method to maximize the gap length under the constraint of cryostat diameter. In this paper, we fixed the gap length to 7 cm because of the constraints from the available bore size of coil and cryostat diameter. We divide the main

and shielding coil by 20 current elements respectively and set the sum of element currents as the objective function to minimize the number of current elements hence the coil size selected as an initial configuration.

Step 1. Determination of coil's initial geometrical configuration and location

We formulated the following linear programing problem to find the coil's initial configuration and location.

Minimize $\sum_{k=1}^{40} | I_k |$

using the element currents as variables

$0 \leq I_1 \sim I_{20} \leq 155$ A

$-155 \leq I_{21} \sim I_{40} \leq 0$ A

under equality constraints to achieve field homogeneity and desired central field

$$\sum_{k=1}^{40} q_2^k = \sum_{k=1}^{40} q_4^k = \sum_{k=1}^{40} q_6^k = \sum_{k=1}^{40} q_8^k = 0$$

Bz(0,0)=1 Tesla

and unequality constraints to restrict the stray field below 5 gauss at a specified distance from the magnet center

| Bz(at z=2m) | $\leq$5 gauss

| Bz(at r=1.5m) | $\leq$5 gauss

We solved this problem using DLPRS subroutine of IMSL (International Mathematical and Statistical Library)[14]. This subroutine is based on the revised simplex algorithm and can solve linear programing problem with linear constraints. Fig. 2 shows optimized distributions of element currents.

Step 2. Optimization of coil's geometrical configuration and location

From the distributions of current elements in Fig. 2, one can see three groups of greater-than-zero current sections in main coil and one group of less-then-zero current sections in shielding coil. These groups can be regarded as individual coils and selected as initial coil configuration as shown in Fig. 3.

In the step 1, we used the operating current of each element as variables but in the step 2, we fixed the operating current to 155 A for main coin and -155 A for shielding coil and used radius R, length L and location S of each coil as variables. We formulated the following nonlinear programing problem to find the optimum coil dimensions.

Minimize the total length of wire

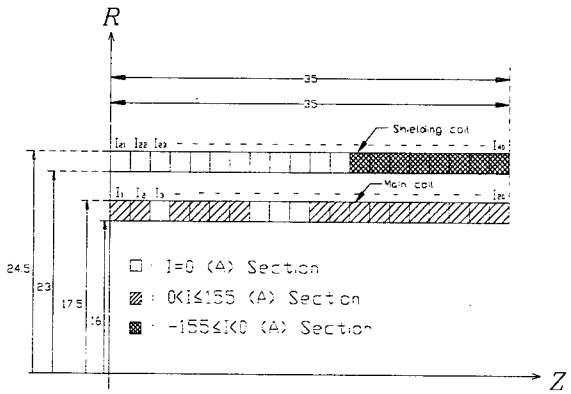

Fig. 2. Optimized distributions of element currents.

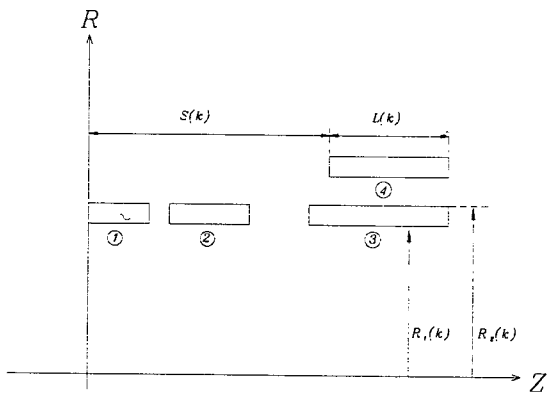

Fig. 3. Initial coil configuration.

$$\sum_{k=1}^{7} \pi \cdot Td \cdot [R_2(k)^2 - R_1(k)^2] \cdot L(k)$$

using the coil size and location as variables

lower limits $\leq X(i) \leq$ upper limits

under equality constraints to achieve field homogeneity and desired central field

$$\sum_{k=1}^{40} q_2^k = \sum_{k=1}^{40} q_4^k = \sum_{k=1}^{40} q_6^k = \sum_{k=1}^{40} q_8^k = 0$$

Bz(0,0) = 1 Tesla

and unequality constraints to restrict the stray field below 5 gauss

| Bz(at z=2m) | $\leq$5 gauss

| Bz(at r=1.5m) | $\leq$5 gauss

where $R_1(k)$, $R_2(k)$, $L(k)$ and Td are inner radius, outer radius, length and turn density of each section respectively. $X(i)$ are $R_2(k)$, $L(k)$ and $S(k)$. We set the total length of wire as the objective function to minimize the amount of conductor hence the cost. For the convenience of fabrication, We fixed the inner radius

Table 1. Optimized coil dimensions (cm).

Section No.	$R_1(k)$	$R_2(k)$	$L(k)$	$S(k)$
1	16(16)	17.1(17.5)	1.68(1.75)	0(0)
2	16(16)	17.1(17.5)	4.2 (3.5)	4.88(5.25)
3	16(16)	17.5(17.5)	9.1 (12.25)	14.98(14)
4	23(23)	24.5(24.5)	6.3 (7)	39.1 (28)

Table 2. Specifications of the main coil and shielding coil.

operating current	main coil : 155 A
	shielding coil : -155 A
central field	1 Tesla
field homogeneity	2.5 ppm/10 cm DSV
stray field	≤ 5 Gauss at 1.8 m on z axis
	≤ 5 Gauss at 1.5 m on r axis
maximum field	1.8 Tesla
conductor	NbTi, 1 mm diameter, 24 filament, Cu:NbTi=7:1, I_c=250 A at 1.8 Tesla
turn density	100 turns/cm^2
length of wire	main coil : 4.2 km
	shielding coil : 2.8 km
inductance	3.6 Henry
stored energy	43.2 kJ

of section 1, 2, 3 to the same value for the convenience of coil fabrication. The outer radius $R_2(k)$ and length $L(k)$ are used as variables which determine coil size. The distance from z=0 plane to the left edge of each section, $S(k)$ are used as variables which define the coil's axial location. We also set simple boundaries on the variables to prevent coil dimensions which are impossible to manufacture(such as the overlapped coil location). We solved this problem using NCONF subroutine of IMSL[14]. This subroutine solve nonlinear programming problem with nonlinear constraints using the successive quadratic programming algorithm and a finite difference gradient. Table 1 lists the optimized dimensions of the main coil and shielding coil. In this table, the data within parenthesis are the initial dimensions and the section numbers are identical with numbers shown in Fig. 3.

Table 2 lists the designed specifications of the main coil and shielding coil. The field homogeneity is 2.5 ppm/10 cm DSV (Diameter of Spherical Volume) and the maximum field inside the coil winding is 1.8 Tesla.

Fig. 4 shows the magnetic field distributions in the central region of the designed coil. Fig. 5 and Fig. 6 shows the magnetic flux distributions of an unshielded coil and an actively shielded coil respectively. As one can see in these figures, the magnetic flux of an unshielded coil stray out infinitely but the magnetic flux of a shielded coil is suppressed by the shielding coil.

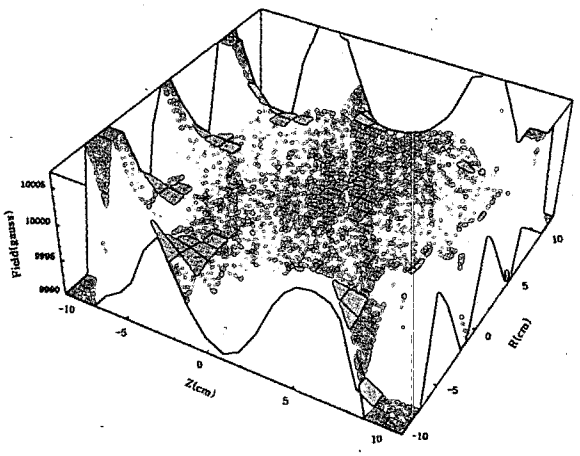

Fig. 4. Magnetic field distributions in central region.

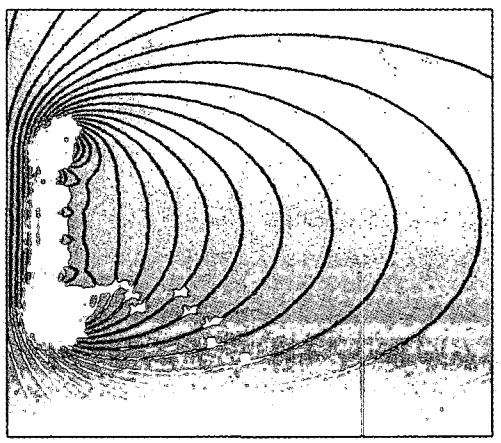

Fig. 5. Magnetic flux distributions of the unshielded coil.

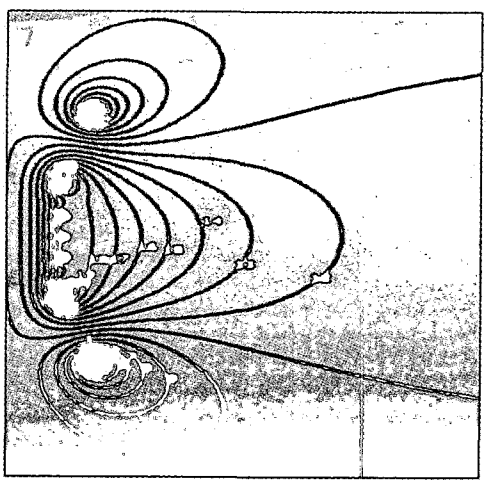

Fig. 6 Magnetic flux distributions of the actively shielded coil.

2. Shim Coil

In the section 2.1, source terms up to the 8th order have been

canceled and thus the 10th order coil has been designed. However, winding errors of a coil and ferromagnetic objects around a magnet generate lower order gradient fields. These lower order gradient fields should be eliminated to achieve required homogeneity of $10^{-5}\sim10^{-6}$. Therefore, a field correction known as shimming is necessary. In this paper, two axial gradient shim coils and two radial gradient shim coils are designed. An important design requirement is that the shims should be orthogonal so that the controls will be independent of each other. This can be achieved if the gradients produced by the various shims are derived from the orthogonal expansion of the spherical harmonics. Equation (1) can be expanded using rectangular coordinates as follows[10];

$$B_z(x,y,z) = A_1^0 + 2A_2^0 Z + 3A_2^1 X + 3B_2^1 Y + 3A_3^0[Z^2-(X^2+Y^2))/2] + 12A_3^1 Z X + 12B_3^1 Z Y + 15A_3^2(X^2-Y^2) + 15B_3^2(2XY) + \cdots \quad (6)$$

where A_1^0 is constant field and the other terms are gradient fields which can be regarded as error fields in MRI magnets. If one designs shim coils to create elementary gradient fields in equation (6), the control of each shim coil will be independent of one another.

Fig. 7 shows the configuration of the first order axial gradient shim coil(z_1 shim coil). This coil must be able to cancel the term $2A_2^0 Z$ in equation (6) without adding other spurious terms. In Fig. 7, one pair of solenoid coils is symmetrically arranged with respect to z=0 plane and fed by opposite currents. This kind of coil arrangement generates only odd order axial gradient fields. The optimum distance and coil size are selected in order that the other odd order gradient fields except the first order should be minimized. We formulated the following nonlinear least squares problem to choose shim coil's configurations.

$$\text{Minimize } \frac{1}{2}\sum_{i=1}^{m} f_i(x)^2$$

$$\text{subject to lower limits} \le X(i) \le \text{upper limits}$$

where $f_i(x)$ are gradient fields to be minimized and $X(i)$ are variables with simple boundaries. The inner radius R_1 of each shim coil is fixed. Outer radius R_2, coil length L and S(distance from z=0 plane to the left edge of each coil) are used as variables.

We solved this problem using BCLSF subroutine of IMSL[14]. Table 3 lists the designed specifications of the z_1 shim coil.

Fig. 8 shows the configuration of the second order axial gradient shim coil(z_2 shim coil). This coil must be able to cancel the term $3A_3^0[Z^2-(X^2+Y^2))/2]$ in equation (6) without adding other spurious terms. In Fig. 8, two pairs of solenoid coils are symmetrically arranged with respect to z=0 plane and fed by opposite current. This kind of coil arrangement generates only even order axial gradient fields. The optimum distance and coil size are selected in order that the other even order gradient fields except

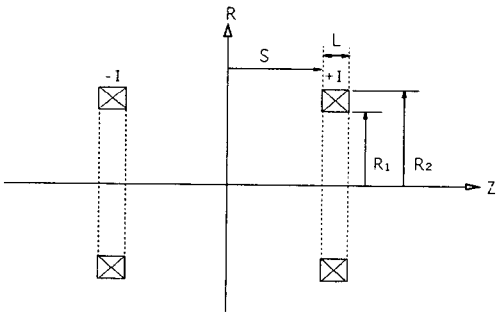

Fig. 7. Configuration of the z_1 shim coil.

Table 3. Specifications of the z_1 shim coil.

R_1 (cm)	R_2 (cm)	L (cm)	S (cm)	Gradient (gauss/cm · A)
24	24.5	1	20.5	6.9×10^{-2}

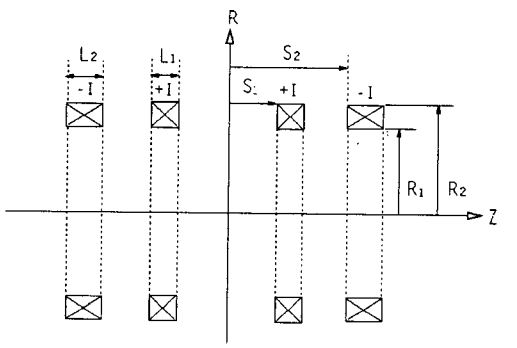

Fig. 8. Configuration of the z_2 shim coil.

Table 4. Specifications of the z_2 shim coil.

R_1 (cm)	R_2 (cm)	L_1 (cm)	L_2 (cm)	S_1 (cm)	S_2 (cm)	Gradient (gauss/cm^2 · A)
24	24.5	0.95	3.2	6.7	27.6	7.5×10^{-3}

the second order should be minimized. Table 4 lists the designed specifications of the z_2 shim coil.

Fig. 9 shows the configuration of the first order radial gradient shim coils(x shim and y shim coil). These coils are designed to cancel the $3A_2^1X$ and $3B_2^1Y$ terms in equation (6) without introducing the other unwanted terms. The x shim coil to eliminate $3A_2^1X$ term can be designed by finding a set of saddle coils such that $\partial^2 Bz/\partial x\partial z=0$ and $\partial^3 Bz/\partial x^3=0$, $\partial^3 Bz/\partial x\partial y^2=0$, $\partial^3 Bz/\partial x\partial z^2=0$. The second derivative can be canceled by placing one pair of saddle coils symmetrically with respect to z=0 plane and applying the same current with respect to z=0 plane and the opposite current with respect to x=0 plane. The third derivatives can be canceled simultaneously by setting the inner angle of saddle coil, θ to 120° and choosing optimum distance S_1 and S_2. The correction of the $3B_2^1Y$ term is carried out by means

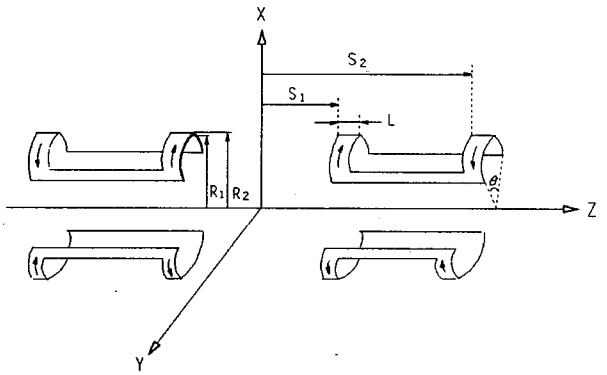

Fig. 9. Configuration of the x shim coil.

Table 5. Specifications of the x and y shim coil.

Coil	R_1 (cm)	R_2 (cm)	L (cm)	S_1 (cm)	S_2 (cm)	Gradient (gauss/cm · A)
X shim	25.5	25.6	2	10	32	2.4×10^{-2}
Y shim	25.65	25.75	2	10	32	2.4×10^{-2}

of the x shim coil rotated 90° around the z axis. Table 5 lists the designed specifications of the first order radial gradient shim coils.

III. Fabrication of Magnet

The coil bobbins were machined from GFRP(Glass Fiber Reinforced Plastic). Great care was taken to position the coil sections correctly according to the designed data in order to achieve the required field homogeneity. The main coil, shielding coil and shim coil were wound from 1 mm diameter NbTi filamentary copper matrix wire. Winding of the coils was carried out on a specially designed winding machine. This winding machine is capable of accurately placing the superconductor onto the coil bobbin. The conductor tensioner was designed so that tension could be maintained on the conductor whether the coil is being wound or unwound. The coils were wound at an even tension using a tension regulator in order to inhibit quenching due to micro-movement of the coil conductors. The layers of the coils were insulated by 0.15 mm thick glass cloth. During winding the tolerances were kept less than 0.05 mm by measuring the dimensions of each layer and correcting the deviations using less or more glass cloth between each layer. After the coils were wound, one layer of copper wire was overbandaged to constrain the outer conductor layers against movement when the magnet is powered up. Fig. 10 shows the wound main coil. Fig. 11 shows the wound shielding coil and axial shim coil. The shielding coil was wound in the opposite direction of the main coil to use the same power supply for energization. The axial shim coils were wound on the same bobbin of the shielding coil. The coil wound on each side of bobbin is shielding coil.

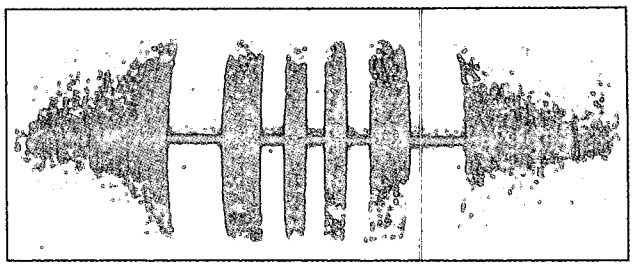

Fig. 10. Main coil.

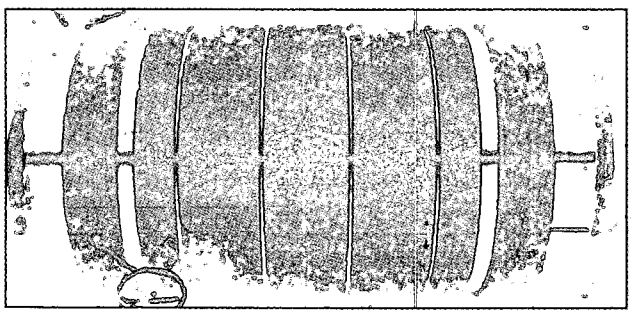

Fig. 11. Shielding coil and axial shim coil.

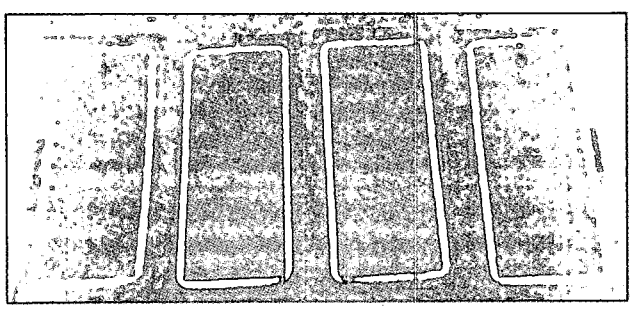

Fig. 12. Radial shim coil.

Radial shim coils were wound on four GFRP plates as shown in Fig. 12. Radial shim coils of saddle type were made by assembling four GFRP plates around the axial shim coils. Fig. 13 shows the assembled radial shim coil. After winding, all coils were assembled for the field test as shown in Fig. 14.

IV. Field Test

The assembled magnet was mounted inside a vertical type cryostat. An insert dewar with 20 cm warm bore was inserted inside the magnet to give room temperature space for measurement. Shim coils were energized up to 5 A to measure field gradients produced by each shim coil. The magnetic field distributions along x, y, z axis were measured by a NMR probe with a resolution of about 10^{-7} Tesla. This NMR probe has the measuring range of 0.7~2.1 Tesla. However, the maximum magnetic fields produced by shim coils are less than 10 Gauss.

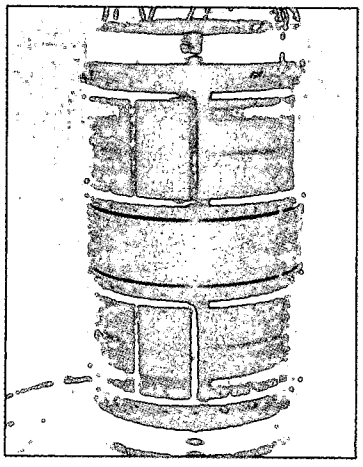

Fig. 13. Assembled radial shim coil.

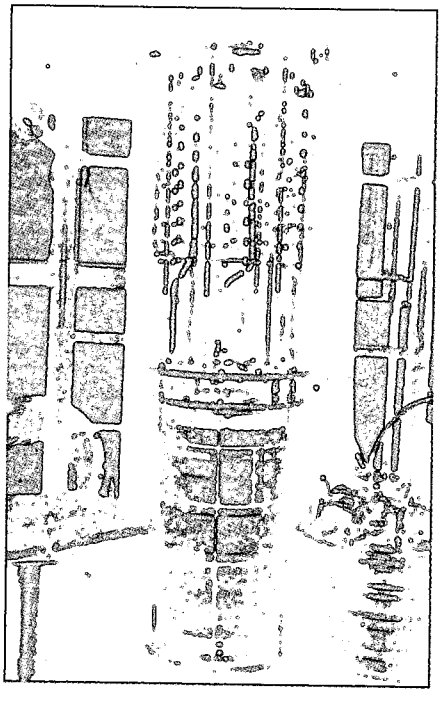

Fig. 14. Magnet assembled with flange.

The magnet was energized up to 155 A by a high stability power supply to produce about 1 Tesla background field so that the magnetic field should be within the measuring range of the NMR probe. First, the magnetic field distributions along x, y, z axis were measured without shim excitation and then combined magnetic field distributions were measured with shim excitation. The magnetic field distributions of only shim coils were calculated by subtracting the former from the latter. Fig. 15, Fig. 16, Fig. 17 and Fig. 18 show the magnetic field distributions of z1, z2, x, y shim coils respectively. Calculated values at 5 A using designed data are showed in the same figure for the comparison with measured values.

Table 6. Gradient of shim coils.

shim coil	gradient per ampere
z_1 shim	7.0×10^{-2} gauss/cm · A
z_2 shim	7.3×10^{-3} gauss/cm^2 · A
x shim	2.7×10^{-2} gauss/cm · A
y shim	2.5×10^{-2} gauss/cm · A

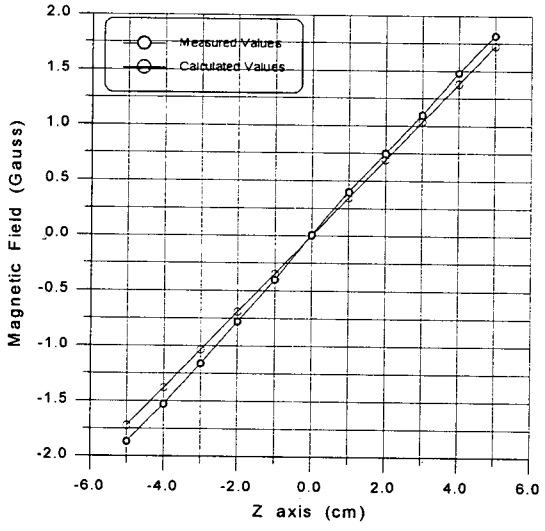

Fig. 15. Magnetic field distribution of z_1 shim coil.

The field distributions of z1 shim coil show the curve of first order function and are good coincidence with calculated values. The field distributions of z2 shim coil show curve of second order function but shift vertically about 0.85 gauss in parallel with calculated values. This shift was caused from the fabrication error of z2 shim coil. The optimum configuration of z2 shim coil was designed so that the other even order gradients(including B_c term)except the second order gradient should be minimized in section 2.2. But the B_c term was not cancelled completely and about 0.85 gauss of B_c term was produced due to fabrication error. However B_c is a constant term and will not deteriorate the field homogeneity when z2 shim coil is energized for the field correction. The field distributions of x, y shim coils show good linearity comparatively.

The gradients produced by each shim coil can be calculated from the data fitting using least square method. Table 6 lists the gradients of each shim coil.

Using the measured magnetic field distributions without shim excitation, the field components of the fabricated magnet were analyzed by data fitting as follows;

$$Bz(z) = 9783.72 + 1.22 \cdot z + 0.23 \cdot z^2 - 8.6\times10^{-4} \cdot z^3 - 1.1\times10^{-3} \cdot z^4 \quad (7)$$

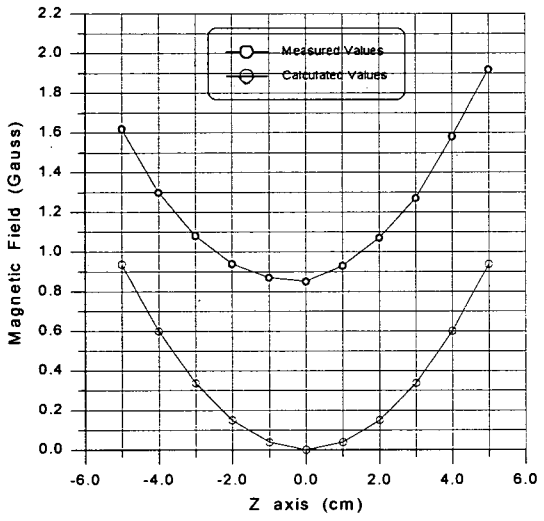

Fig. 16. Magnetic field distribution of z_2 shim coil.

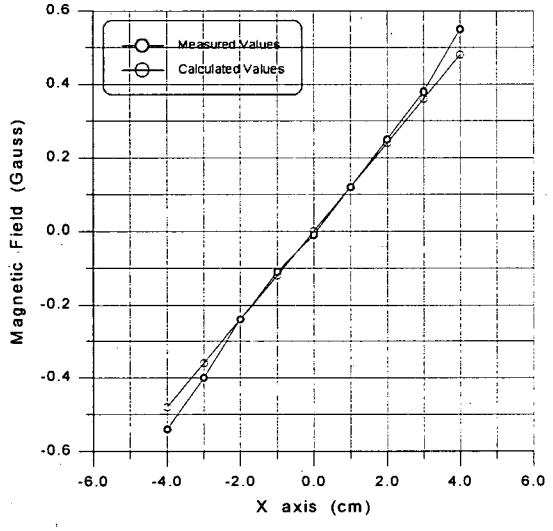

Fig. 17. Magnetic field distribution of x shim coil.

$$Bz(x) = 9783.74 + 0.07 \cdot x - 0.1 \cdot x^2 - 3\times10^{-4} \cdot x^3 - 3\times10^{-4} \cdot x^4 \quad (8)$$

$$Bz(y) = 9783.7 - 0.13 \cdot y - 0.12 \cdot y^2 + 9.1\times10^{-4} \cdot y^3 + 4.6\times10^{-4} \cdot y^4 \quad (9)$$

The magnetic field homogeneity within 10cm along z axis is 1300 ppm without shim excitation. It is 520 times higher than designed data. This inhomogeneity is mainly due to first and second order gradient fields as one can see in equation (7).

The operating current of z1 shim coil to cancel the first order gradient field can be calculated by dividing the coefficient of first order gradient field in equation (7) by gradient of z1 shim coil given in table 6 as below.

$$-\frac{1.22\ \ gauss/cm}{7.0\times10^{-2}\ \ gauss/cm \cdot A} = -17.4\ A$$

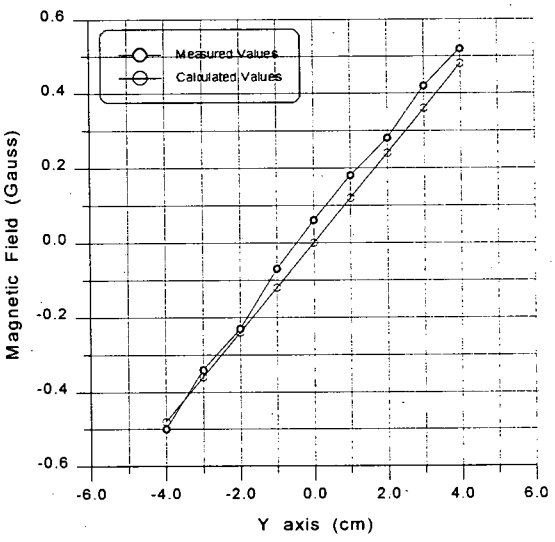

Fig. 18. Magnetic field distribution of y shim coil.

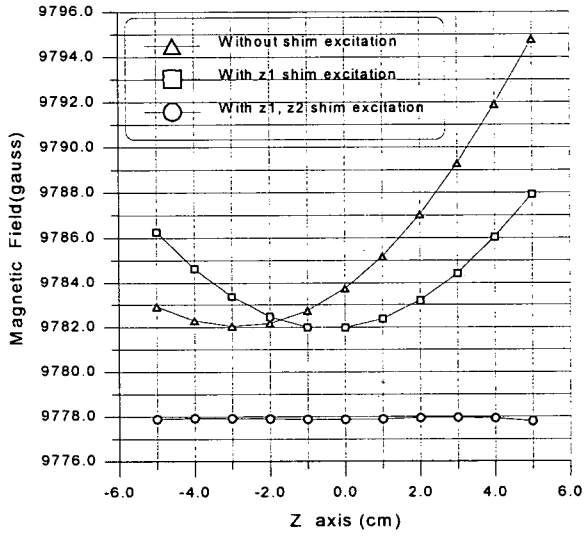

Fig. 19. Magnetic field distribution along z axis.

The operating current of z2 shim coil to cancel the second order gradient was calculated as -31.5 A. Fig. 19 shows the magnetic field distributions along z axis before and after correction using shim coils. The magnetic field homogeneity within 10cm along z axis was improved to 15ppm by correction using z_1 and z_2 shim coils.

Before field correction, the magnetic field homogeneity within 8cm along x, y axis are 200ppm and 236ppm respectively. The operating current of x and y shim coil to cancel the first order gradient field was calculated as -2.6 A and +5.24 A respectively. Fig. 20 and Fig. 21 show the magnetic field distributions along x, y axis before and after correction. After correction using x, y shim coil, the magnetic field homogeneity within 8cm along x, y axis became 170ppm and 189ppm respectively. The homogeneity

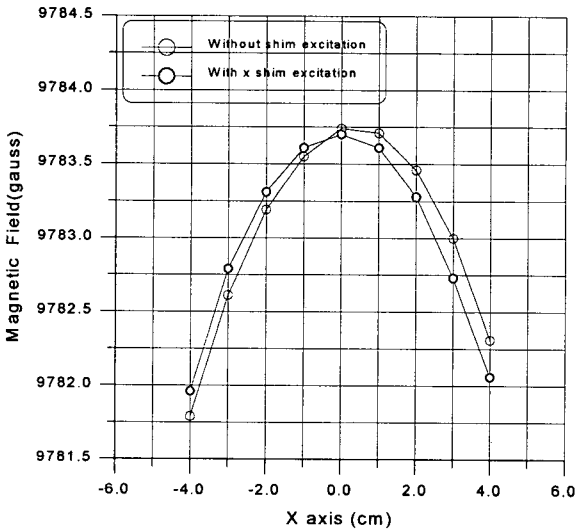

Fig. 20. Magnetic field distribution along x axis.

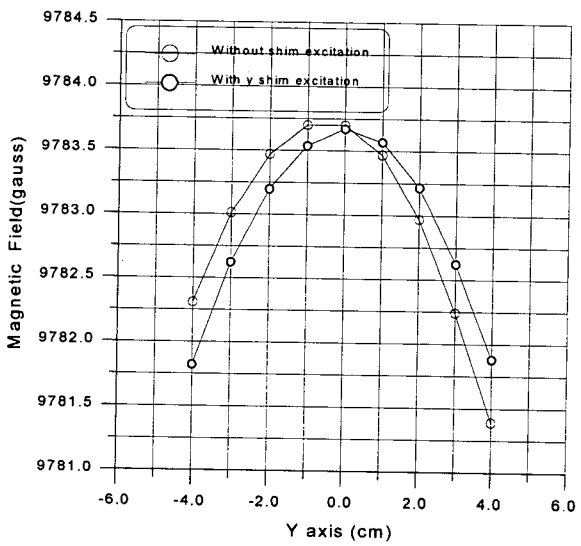

Fig. 21. Magnetic field distribution along y axis.

was not much improved by correction using x, y shim coil. The inhomogeneity along x, y axis is mainly due to second order gradients as one can see in Fig. 20 and Fig. 21. Second order radial shim coils should be added to improve the field homogeneity.

The stray field distributions were measured by a Hall probe to confirm the shielding effect. Fig. 22 shows the 5 Gauss stray field contours of 1 Tesla magnet with and without shielding coil. The 5 Gauss field points of the magnet without shielding coil are located at 270 cm axially and 210 cm radially from the magnet center. However, the 5 Gauss field points of the magnet are reduced to 175 cm axially and 148 cm radially by shielding coil. The volume enclosed by the 5 Gauss stray field contour is reduced from 75 m^3 to 24 m^3 by the shielding effect of shielding coil.

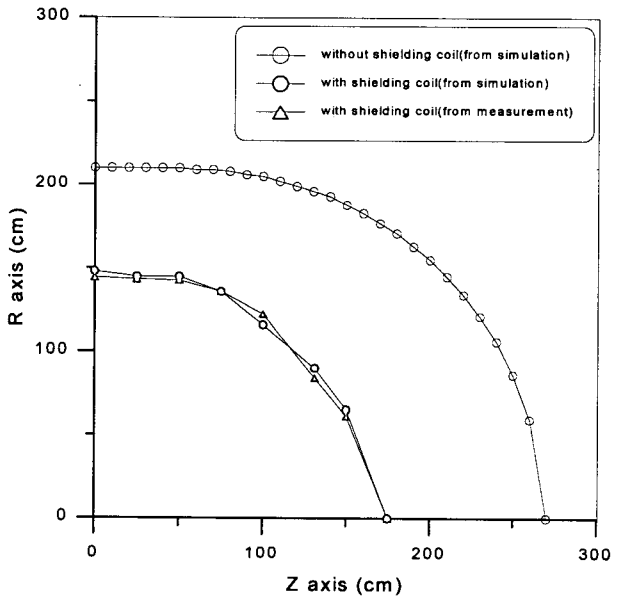

Fig. 22. The 5 Gauss stray field contours.

V. Conclusions

MRI system is a high performance diagnostic instrument and has good resolution at a high magnetic field. Magnet generating high magnetic field will produce strong stray fields. A well designed magnetic shield can eliminate the drawbacks arising from the strong stray field. We have developed the computer optimization program for the design of actively shielded MRI magnet. The actively shielded superconducting MRI magnet with a small warm bore was fabricated and four sets of superconducting shim coils were equipped. The magnetic field distributions were measured and field correction was carried out using shim coils. According to the test results, we could confirm the usefulness of the computer program and magnet fabrication techniques developed in this study.

References

[1] D. C. Hawksworth, "Development of Superconducting Magnet Systems for MRI", Advances in Cryogenic Engineering, Vol. 35, pp. 529-538, 1990.

[2] H. Siebold, "Performance and Results of a Computer Program for Optimizing Magnet with Iron", IEEE Transactions on Magnetics, Vol. 24, No. 1, pp. 419-422, 1988.

[3] Y. Shimada, et al., "Superconducting Magnet with Self-Shield for Whole Body Magnetic Resonance Imaging", IEEE Transactions on Magnetics, Vol. 27, No. 2, pp. 1685-1688, 1991.

[4] M. D. Ogle, et al., "Design Optimization Method for a Ferromagnetically Self-Shield MR Magnet", IEEE Tran-

sactions on Magnetics, Vol. 27, No. 2, pp. 1689-1691, 1991.

[5] R. Morad, et al., "The Design and Use of Secondary Shielding in MRI Systems-Experience from 4 Years of Operation", IEEE Transactions on Magnetics, Vol. 24, No. 2, pp. 1288-1291, 1988.

[6] D. G. Hawksworth, et al., "Considerations in the Design of MRI Magnets with Reduced Stray Fields", IEEE Transactions on Magnetics, Vol. 23, No. 2, pp. 1309-1314, 1987.

[7] F. J. Davies, et al., "A 2-Tesla Active Shield Magnet for Whole Body Imaging and Spectroscopy", IEEE Transactions on Magnetics, Vol. 27, No. 2, pp. 1677-1680, 1991.

[8] M. Fujita, "The Coil Design of the Superconducting MRI Magnet", IEEE Transactions on Magnetics, Vol. 24, No. 6, pp. 2907-2909, 1988.

[9] A. K. Kalafala, "Optimized Configurations for Actively Shielded Magnetic Resonance Imaging Magnets", IEEE Transactions on Magnetics, Vol. 27, No. 2, pp. 1696-1699, 1991.

[10] W. A. Anderson, "Electrical Current Shims for Correcting Magnetic Fields", The Review of Scientific Instruments, Vol. 32, No. 3, pp. 241-250, 1961.

[11] V. B. Nazarov, et al., "Compensators for Non-uniformity of the magnetic Field of a Superconducting Solenoid", Cryogenics, December, pp. 470-471, 1972.

[12] M. D. Sauzade and S. K. Kan, "High Resolution Nuclear Magnetic Resonance Spectroscopy in High Magnetic Fields", Advances in Electronics and Electron Physics, Academic Press. pp. 1-93, 1974.

[13] F. Romeo, et al,. "Magnetic Field Profiling: Analysis and Correcting Coil Design", Magnetic Resonance in Medicine 1, pp. 44-65, 1984.

[14] IMSL MATH/LIBRARY, IMSL, Inc., Version 1. 1, 1989.

Hong-Beom Jin was born in Nov. 20, 1962. He received the B.S. degree in electrical engineering from Sung Kyun Kwan University in 1987. He received the M.S. degree in electrical engineering from Sung Kyun Kwan University in 1989. He received the Ph.D. degree in electrical engineering from Sung Kyun Kwan University in 1997. He has been with the Applied Superconductivity Lab. of Korea Electrotechnology Research Institute since 1991 where he is now a senior researcher. His research activities are in the areas on superconductor application.

Kang-Sik Ryu was born in Aug. 20, 1956. He received the B.S. degree in electrical engineering from Han Yang University in 1980. He received the M.S. degree in electrical engineering from Kwang Woon University in 1984. He received the Ph.D. degree in electrical engineering from Han Yang University in 1987. He has been with Applied Superconductivity Lab. of Korea Electrotechnology Research Institute since 1988 where he is now a head of Applied Superconductivity Lab.. His research activities are in the areas on superconductor application.

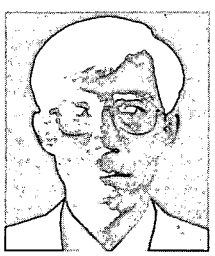

Bong-Hwan Oh was born in 1959. He received the B.S. and M.S. degrees in electrical engineering from MyongJi University in 1985 and 1987 respectively. He received the Ph.D. degrees in electrical engineering from Nagoya University, Nagoya, Japan, in 1993. He joined the Korea Elelctrotechnology Research Institute as a senior researcher in 1994, where he remained until January, 1997. And, currently, he joined the Department of Electrical Engineering MyongJi College as an assistant professor. His research interests are application of superconducting technology. Dr. Oh is a member of the KIEE, JIEE and Cryogenic Engineering of Japan.

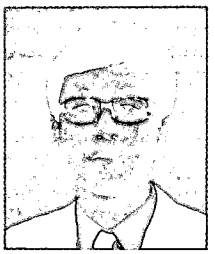

Kyung-Woo Ryu was borin in Andong, Korea, on Feb. 10, 1962. He received the B.S. degree in electrical engineering from Inha University, Inchon, Korea in 1983, the M.S. degree in electrical engineering from Seoul National University, Seoul, Korea in 1985, and the Ph.D. degree in electrical and computer engineering from Yokohama National University, Yokohama, Japan in 1995, respectively. He was with Applied Superconductivity Lab. of Korea Electrotechnology Research Institute from 1986 to 1995, where he was a senior researcher. He has been with the department of electricl engineering at Chonnam National University since 1996 where he is now a lecturer. His research activities are in the areas on superconductor applications.

In-Young Jeong was born in Korea. He received the B.S. degree in electrical engineering in 1979 from Chung-buk National University, Korea, and the M.S. and Ph.D. degrees in electrical engineering from Sung-kyun-kwan University, Korea, in 1985 and 1990, respectively. He has been with the department of electrical Engineering at Doo-won Technical College, since 1994, where he is an associate Professor. His research interests are in the area of the piezoelectric ceramic filter and the sensor engineering.